Electrical enhancement period of solar photovoltaic using phase change material

Sourav Khanna[a,*], Sanjeev Newar[b], Vashi Sharma[c], K. S. Reddy[d], Tapas K. Mallick[e,*], Jovana Radulovic[f], Rinat Khusainov[g], David Hutchinson[h], Victor Becerra[a]

[a] School of Energy and Electronic Engineering, University of Portsmouth, Portsmouth PO1 3DJ, United Kingdom

[b] Department of Industrial and Management Engineering, IIT Kanpur, India

[c] Department of Mechanical Engineering, IIT Kanpur, India

[d] Department of Mechanical Engineering, IIT Madras, India

[e] Environment and Sustainability Institute, Penryn Campus, University of Exeter, United Kingdom

[f] School of Mechanical and Design Engineering, University of Portsmouth, Portsmouth PO1 3DJ, United Kingdom

[g] School of Computing, University of Portsmouth, Portsmouth PO1 3DJ, United Kingdom

[h] Faculty of Technology, University of Portsmouth, Portsmouth PO1 3AH, United Kingdom

Abstract

Temperature management in photovoltaic (PV) is critical for the power output. Phase Change Material (PCM) usage enables one to remove heat from the system and achieve enhanced electrical output. This study aims at finding the period of PV electrical enhancement, the increase in power and increase in electrical efficiency achieved using PCM under different working circumstances. Results suggest that as the angle of approach of wind changes from 75° to 0°, the electrical enhancement period elevates from 7.0 h to 8.6 h for 5 cm deep PCM box. But, the increase in power drops from 17.6 W/m^2 to 13.6 W/m^2. As wind speed changes from 6 m/s to 0.2 m/s, the electrical enhancement period drops from 9.1 h to 6.4 h. But, the increase in power rises from 11.8 W/m^2 to 22.8 W/m^2. The rise in ambient temperature 289 K to 299 K leads to decrement of electrical enhancement period from 12.6 h to 7.1 h. But the increase in power rises from 15.9 W/m^2 to 21.4 W/m^2. Elevation in temperature for liquification from 291 K to 301 K leads to increment of electrical enhancement period from 6.5 h to 12.3 h.

* Corresponding Authors

Email: sourav.khanna@port.ac.uk (Sourav Khanna)

t.k.mallick@exeter.ac.uk (Tapas K. Mallick)

1. Introduction

1.1 Motivation

Temperature management in photovoltaic is critical for the power output. Phase Change Material usage enables one to remove heat from the system and achieve enhanced electrical output.

1.2 Literature Review

Experiments have been performed on PV in Tehran using PCM by Baygi and Sadrameli (2018). The setup witnesses the PV temperature drop of 15°C against the case of no PCM where the temperature rises till 60°C. The impact of different climates of Vehari and Dublin using PCM discussed by Hasan et al. (2015). The respective PV temperature drops attained in two cases are reported as 21.5°C and 10°C. Experiments on a virtual PV with paraffin wax as coolant have been reported by Huang et al. (2006, 2007). It has also been concluded that the fins in the PCM can cause even more cooling. Lu et al. (2018) have also analysed the fins in the PCM for the cooling of building integrated concentrating photovoltaic and found a 12% improvement in electrical efficiency. Comparison between two different setups has been carried out by Indartono et al. (2014) for Indonesia. Same PCM is filled on back sides of a) PV inclined at a support, and b) PV placed in touch with roof. The respective cooling is reported as 2.6°C and 5.7°C. Hasan et al. (2010) have compared PCMs amongst a range for their performances in terms of cooling. The authors have reported the highest cooling of 18°C in case of PCMs: CP-acid and $CaCl_2H_{12}O_6$. Kamkari and Groulx (2018) have discussed the dynamics of lauric acid-PCM during melting when heated from rear. The melting rate of PCM is found to be fastest when box is kept grounded rather than standing or slanted. Zhang et al. (2018) have reported a review study on the use of solid-liquid PCM for the thermal energy storage. An innovative kind of PCM, infused with nano-particles is studied by Sharma et al. (2017). Waqas et al. (2017) have equipped the PV with PCM filled metallic tubes. Indian state of Punjab has been chosen by Preet et al. (2017) to carry out experimental study using paraffin wax 30 as PCM. The PV temperature has been recorded to have come down by an effective 25°C. Browne et al. (2015, 2016) have performed experiments with a differently synthesised compound constituting various materials that are chemically inert to each other. Different fatty acids are used to form the desired PCM that have caused temperature drop of 5.5°C. Tracking setups with paraffin wax as PCM have been experimentally monitored by Su et al. (2018) in Macau and an effective enhancement of 10% in electrical output has been achieved. Siyabi et al. (2018a, 2018b) have used multiple PCM heat sink and stacked heat sink for the purpose of thermal management.

Brano et al. (2014) have simultaneously studied the impact of time and space using forward and central difference models respectively using paraffin wax 27 as PCM. The approach is used to compare computational and experimental results. The comparison testifies correctness of the approach as the difference does not exceed -6.5°C and 7.5°C on either side. Kant et al. (2016) have studied the paraffin wax 35 PCM using conduction-alone model and conduction-convection model. The respective PV cooling is reported as 1.5°C and 5°C. Graphite with permeating PCM is used by Atkin and Farid (2015) and an improvement of 7% is observed in power output. Implicit method to model enthalpy has been applied by Kibria et al. (2016) for comparing variants of paraffin wax viz. 20, 25, and 28. Paraffin wax 20 is found to have liquefied at fastest rate among all three. Ma et al. (2018) have performed the sensitivity analysis of PV-PCM system. Benlekkam et al. (2018) have studied the impact of tilt of fins on the performance of PV-PCM. Biwole et al. (2013, 2018) have studied the PCM domain with suitable modelling by emphasizing on the elimination of the cases leading to divergence. The optimum values for the liquification temperature of PCM have been reported for PV-PCM and PVT-PCM systems by Park et al. (2014) and Su et al. (2017) respectively. Khanna et al.

(2018a, 2018b) have investigated the impact of climates on the contribution of PCM in PV cooling and carried out the optimization (Khanna et al., 2018c; 2018d; 2019). Arici et al. (2018) have also carried out the optimization of PV-PCM system. Khanna et al. (2018e) have studied PV-PCM system for Cornwall. Various alignments of heat-exchangers transferring heat to PCM are investigated by Emam and Ahmed (2018) and parallel alignment is reported as best. Computational results for a virtual PV with paraffin wax as coolant have been reported by Huang et al. (2004, 2011). It has been concluded that the fins in the PCM can cause further cooling. Emam et al. (2017) and Khanna et al. (2017a) have investigated CPV-PCM and PV-PCM when heated from front. The PCM's melting rate was found to be fastest when box was kept standing or slanted rather than grounded. The adoption of analytical expressions (Khanna et al., 2014; 2016; Khanna and Sharma, 2015; 2016; Sharma et al. 2016) can ease the calculations in the domain of PV-PCM thermal analysis. Sathe and Dhoble (2018) have used extended surfaces in the PCM to enhance the cooling of CPV.

1.3 Contribution

In the current work, the period of PV electrical enhancement, the increase in power and increase in electrical efficiency achieved using PCM under different working circumstances are reported.

2. Physical Model

PV and PV-PCM having an inclination angle of β are considered (Fig. 1). Dimensions of PCM box are L and d respectively.

The presented study is applicable within the following suppositions

(i) Solar energy density is similar over the surface of PV

(ii) Outer surfaces of PCM box are kept thermally isolated from ambient

(iii) Properties of PV, solidus PCM and liquidus PCM are unaltered across directions and space

(iv) PV is constructed by coupling 5 different coverings and thermal resistances in between the coverings are neglected

3. Mathematical Modelling

The solar irradiance soaked up by PV that does not take part in electricity generation leads to thermal energy production. It has been articulated as

$$E = \left[(\tau\alpha)_c\, S - \eta_{STC} S \left\{1 + \beta_c (T_{PV} - 25) + \gamma_c \ln\left(\frac{S}{1000}\right)\right\}\right] / t_{si} \tag{1}$$

The initial term of the aforementioned equation covers the solar irradiance soaked up by PV and latter term covers the power production that takes into account the impact of PV temperature and intensity of solar irradiance. A part of the thermal energy dissipates radiatively and convectively from the top and back. Forced part of convective mode is articulated by taking into account the impact of wind speed (s_w) and angle of approach of wind (γ_w) for top (h_t) and back (h_b) as (Kaplani and Kaplanis, 2014)

$$h_t = 0.848\, k_a [\sin\beta \cos\gamma_w\, \mathrm{s}_w\, \mathrm{Pr}/\upsilon]^{1/2} (L_{ch}/2)^{-1/2} \tag{2}$$

$$h_b = \begin{cases} 3.83\, \mathrm{s}_w{}^{0.5}\, L_{ch}{}^{-0.5} & for\ laminar\ flow \\ 5.74\, \mathrm{s}_w{}^{0.8}\, L_{ch}{}^{-0.2} - 16.46\, L_{ch}{}^{-1} & for\ mixed\ flow \\ 5.74\, \mathrm{s}_w{}^{0.8}\, L_{ch}{}^{-0.2} & for\ fully\ turbulent\ flow \end{cases} \tag{3}$$

Natural part of convective mode is articulated by using Nusselt number for top (Nu_t) and back (Nu_b) as (Kaplani and Kaplanis, 2014; Khanna et al., 2017)

$$Nu_t = \begin{cases} [0.13(PrGr)^{0.33}] & for\ \beta \le 30° \\ [0.13\{(PrGr)^{0.33} - (PrGr_c)^{0.33}\} + 0.56(PrGr_c \sin\beta)^{0.25}] & for\ \beta > 30° \end{cases} \tag{4}$$

$$Nu_b = \begin{cases} 0.58(Ra)^{0.2}; & for\ \beta \leq 2° \\ 0.56(Ra\sin\beta)^{0.25}; & for\ 2° < \beta < 30° \\ \left[0.825 + \dfrac{0.387(Ra\sin\beta)^{0.1667}}{\{1+(0.492/Pr)^{0.5625}\}^{0.2963}}\right]^2 & for\ \beta \geq 30° \end{cases} \quad (5)$$

3.1 Solid Components

The energy balance for the ith layer of the solid components can be written as

$$\rho_i C_{p,i}\frac{\partial T_i}{\partial t} = \nabla.(k_i \nabla T_i) + E_i \quad (6)$$

with below boundaries

$$k_i\frac{\partial T_i}{\partial y} = h_c[T_i - T_a] + F_{t\_sk}\sigma\varepsilon_t[T_t^4 - T_{sk}^4] + F_{t\_gr}\sigma\varepsilon_t[T_t^4 - T_{gr}^4] \qquad at\ top \quad (7)$$

$$k_i\frac{\partial T_i}{\partial x} = 0 \quad at\ edges \quad (8)$$

$$k_i\frac{\partial T_i}{\partial y} = k_{i+1}\frac{\partial T_{i+1}}{\partial y} \quad at\ interface \quad (9)$$

$$k_i\frac{\partial T_i}{\partial y} = h_c[T_i - T_a] + F_{re\_sk}\sigma\varepsilon_{re}[T_i^4 - T_{sk}^4] + F_{re\_gr}\sigma\varepsilon_{re}[T_i^4 - T_{gr}^4] \qquad at\ rear \quad (10)$$

$$T_i = T_a\ when\ t = 0 \quad (11)$$

Eq. (7) covers the convective energy loss from top to the ambient, radiative energy loss from top to the sky and from top to ground. Both forced (Eq. 2) and natural (Eq. 4) modes of convective energy flow are considered. Eq. (8) covers no heat loss condition at the edges.

3.2 Phase Change Material

The energy/momentum/mass balances for the PCM can be written as

$$\rho_P C_p\frac{\partial T_P}{\partial t} = \nabla.(k_P \nabla T_P) - \rho_P C_{p,P}(\vec{v}.\nabla T_P) \quad (12)$$

$$\rho_P\frac{\partial v_x}{\partial t} + \rho_P v_x\frac{\partial v_x}{\partial x} + \rho_P v_y\frac{\partial v_x}{\partial y} = -\frac{\partial p}{\partial x} + \mu_{P,l}\nabla^2\vec{v} + \rho_{P,l}g_x[1 - \beta_c(T_P - T_m)] - F_x \quad (13)$$

$$\rho_P \frac{\partial v_y}{\partial t} + \rho_P v_x \frac{\partial v_y}{\partial x} + \rho_P v_y \frac{\partial v_y}{\partial y} = -\frac{\partial p}{\partial x} + \mu_{P,l} \nabla^2 \vec{v} + \rho_{P,l} g_y [1 - \beta_c (T_P - T_m)] - F_y \quad (14)$$

$$\nabla . \vec{v} = 0 \quad (15)$$

with below boundaries

$$k_P \frac{\partial T_P}{\partial y} = k_{al} \frac{\partial T_{al}}{\partial y} \; for\ aluminium - PCM\ interface\ along\ length \quad (16)$$

$$k_P \frac{\partial T_P}{\partial x} = k_{al} \frac{\partial T_{al}}{\partial x} \; for\ aluminium - PCM\ interface\ along\ depth \quad (17)$$

$$T_P = T_a \;\; when\ t = 0 \quad (18)$$

$$v_x = v_y = 0\ at\ inner\ surface\ of\ PCM\ box \quad (19)$$

$$v_x = v_y = 0\ when\ t = 0 \quad (20)$$

ANSYS Fluent 17.1 is used to solve the above equations.

4. Experimental Validation

Experimentations to study the photovoltaic with phase change material are carried out (Hasan et al., 2015). To establish the precision of the current model by comparing the computed results with experimental observations, the analysis is carried out using same system. The computed values of the average PV temperature are put against the experimental observations in Figure 2. The results suggest that the both match satisfactorily.

5. Results and Discussion

The period of electrical enhancement, power production, electrical efficiency, increase in electrical efficiency and increase in power have been computed. The specifications are presented by Khanna et al. (2019).

5.1 Period of Electrical Enhancement and Increase in Power

5.1.1 Impact of Wind Speed

The period of electrical enhancement of PV has been computed for a span of wind speed and deepness of PCM box and plotted in Figure 3. The results show that as wind speed drops from 6 m/s to 5 m/s, 4 m/s, 3 m/s, 2 m/s, 1 m/s and 0.2 m/s, the electrical enhancement period decreases from 9.1 h to 8.8 h, 8.5 h, 8.0 h, 7.5 h, 6.9 h and 6.4 h respectively for 5cm deep PCM box. The reason can be explained as follows. The low wind speed drops the thermal loss and increases the heat collection rate by PCM that increases the speed of liquification and, thus, drops the period of electrical enhancement.

The electricity generation and electrical efficiency have been computed for a span of wind speed and plotted in Figures 4 and 5. The results show that as wind speed drops from 6 m/s to 5 m/s, 4 m/s, 3 m/s, 2 m/s, 1 m/s and 0.2 m/s, the electricity generation decreases from 191.3 to 191.0, 190.4, 189.6, 188.5, 187.0 and 185.4 W/m^2 respectively. The reason can be explained as follows. The low wind speed decreases the heat losses from the PV which leads to increase in the PV temperature resulting in decrease in the electricity generation.

The increase in power and electrical efficiency achieved by PCM have been computed for a span of wind speed and plotted in Figures 4 and 5. The results show that as wind speed drops from 6 m/s to 5 m/s, 4 m/s, 3 m/s, 2 m/s, 1 m/s and 0.2 m/s, the increase in power elevates from 11.8 to 12.4, 13.6, 15.0, 17.0, 19.8 and 22.8 W/m^2 respectively. The reason can be explained as follows. The high wind speed takes away the PV's heat efficiently and cools the PV which decreases the contribution of phase change material in PV cooling.

5.1.2 Impact of Angle of Approach of Wind

The period of electrical enhancement of PV has been computed for a span of angle of approach of wind and deepness of PCM box and plotted in Figure 6. The results show that as the angle of approach of wind decreases from 75° to 60°, 45°, 30°, 15° and 0°, the electrical enhancement period increases from 7.0 h to 7.6 h, 8.0 h, 8.3 h, 8.5 h and 8.6 h for 5 cm deep PCM box. The reason can be explained as follows. When wind approaches normally to PV, it takes away the PV's heat efficiently that reduces the rate of heat collection by PCM and reduces the speed of liquification and, thus, increases the period of electrical enhancement.

The electricity generation and electrical efficiency have been computed for a span of angle of approach of wind and plotted in Figures 7 and 8. The results show that as the angle of approach of wind decreases from 75° to 60°, 45°, 30°, 15° and 0°, the electricity generation increases from 189.2 to 189.7, 190.0, 190.2, 190.3 and 190.4 W/m^2 respectively. The reason can be explained as follows. When wind approaches normally to PV, it takes away the PV's heat efficiently which leads to decrease in the PV temperature resulting in increase in the electricity generation and the electrical efficiency.

The increase in power and electrical efficiency achieved using PCM have been computed for a span of angle of approach of wind and plotted in Figures 7 and 8. The results show that as the angle of approach of wind decreases from 75° to 60°, 45°, 30°, 15° and 0°, the increase in power reduces from 17.6 to 15.9, 14.8, 14.1, 13.7 and 13.6 W/m^2 respectively. It is because the low wind azimuth angle increases the heat losses from the PV and cools the PV which decreases the contribution of phase change material in PV cooling.

5.1.3 Impact of Surroundings Temperature

The period of electrical enhancement of PV has been computed for a span of surroundings temperature and deepness of PCM box and plotted in Figure 9. The results show that as the surroundings temperature increases from 289 K to 291 K, 293 K, 295 K, 297 K and 299 K, the electrical enhancement period drops from 12.6 h to 10.9 h, 9.6h, 8.6 h, 7.7 h and 7.1 h respectively for 5 cm deep PCM box. The reason can be explained as follows. For the case of higher surrounding temperature, the rate of heat collection by PCM rises that increases the speed of liquification and, thus, drops the period of electrical enhancement.

The electricity generation and electrical efficiency have been computed for a span of surroundings temperature and plotted in Figures 10 and 11. The results show that as the surroundings temperature increases from 289 K to 291 K, 293 K, 295 K, 297 K and 299 K, the electrical generation drops from 194.8, 192.8, 190.9, 188.9, 186.9 and 185.0 W/m^2. It is because for the case of higher surrounding temperature, the PV temperature rises which leads to decrease in the electricity generation and electrical efficiency.

The increase in power and electrical efficiency achieved using PCM have been computed for a span of surroundings temperature and plotted in Figures 10 and 11. The results show that as surroundings temperature increases from 289 K to 291 K, 293 K, 295 K, 297 K and 299 K, the increase in power elevates from 15.9 to 17.0, 18.1, 19.2, 20.3 and 21.4 W/m^2 respectively. It is because the low surrounding temperature keeps the PV operating temperature low which decreases the contribution of phase change material in PV cooling.

5.1.4 Impact of PCM Liquification Temperature

The period of electrical enhancement of PV has been computed for a span of PCM liquifiction temperature and deepness of PCM box. The results (Fig. 12) suggest that as the temperature for liquification increases from 291 K to 293 K, 295 K, 297 K, 299 K and 301 K, the electrical enhancement period elevates from 6.5 h, 7.3 h, 8.2 h, 9.3 h, 10.7 h and 12.3 h respectively for 5 cm deep PCM box. The reason can be explained as follows. The lesser temperature of liquification helps the photovoltaic to operate at lesser temperature which leads to decrement in the losses to surroundings and, consequently, increment in the rate of heat collection by phase change material and increase in the speed of liquification and, thus, drops the period of electrical enhancement.

6. Conclusions

The study aims at finding the period of PV electrical enhancement, electricity generation, electrical efficiency and increase in power achieved using PCM for a span of wind speed, angle of approach of wind, surrounding temperature and PCM liquification temperature. Results suggest that

(i) As wind speed drops from 6 m/s to 5 m/s, 4 m/s, 3 m/s, 2 m/s, 1 m/s and 0.2 m/s, the electrical enhancement period decreases from 9.1 h to 8.8 h, 8.5 h, 8.0 h, 7.5 h, 6.9 h and 6.4 h respectively for 5 cm deep PCM box.

(ii) As the angle of approach of wind decreases from 75° to 60°, 45°, 30°, 15° and 0°, the electrical enhancement period increases from 7.0 h to 7.6 h, 8.0 h, 8.3 h, 8.5 h and 8.6 h.

(iii) As the surroundings temperature increases from 289 K to 291 K, 293 K, 295 K, 297 K and 299 K, the electrical enhancement period drops from 12.6 h to 10.9 h, 9.6h, 8.6 h, 7.7 h and 7.1 h.

(iv) As the temperature for liquification increases from 291 K to 293 K, 295 K, 297 K, 299 K and 301 K, the electrical enhancement period elevates from 6.5 h, 7.3 h, 8.2 h, 9.3 h, 10.7 h and 12.3 h.

Acknowledgment

Funding from EPSRC-DST funded Reliable and Efficient System for Community Energy Solution - RESCUES project (EP/K03619X/1) and UKIERI-DST2016-17-0089 project to the University of Exeter and Indian Institute of Technology, Madras is greatly acknowledged. The University of Portsmouth has received funding from the Interreg 2 Seas programme 2014-2020 co-funded by the European Regional Development Fund under subsidy contract No 2S04-004.

References

Arici M., Bilgin F., Nizetic S., Papadopoulos A.M., 2018. Journal of Cleaner Production 189, 738-745.

Atkin P., Farid M.M., 2015. Solar Energy 114, 217–228.

Baygi S.R.M., Sadrameli S.M., 2018. Thermal Science and Engineering Progress 5, 405–411.

Benlekkam M.L., Nehari D., Madani H.I., 2018. International Journal of Heat and Technology 36 (3), 919-926.

Biwole P.H., Eclache P., Kuznik F., 2013. Energy and Buildings 62, 59–67.

Biwole P.H., Groulx D., Souayfane F., Chiu T., 2018. International Journal of Thermal Sciences 124, 433-446.

Brano V.L., Ciulla G., Piacentino A., Cardona F., 2014. Renewable Energy 68, 181–193.

Browne M.C., Lawlor K., Kelly A., Norton B., McCormack S.J., 2015. Energy Procedia 70, 163–171.

Browne M.C., Norton B., McCormack S.J., 2016. Solar Energy 133, 533–548.

Emam M., Ahmed A., 2018. Energy Conversion and Management 158, 298–314.

Emam M., Ookawara S., Ahmed M., 2017. Solar Energy 150, 229–245

Hasan A., McCormack S.J., Huang M.J., Norton B., 2010. Solar Energy 84, 1601–1612.

Hasan A., McCormack S.J., Huang M.J., Sarwar J., Norton B., 2015. Solar Energy 115, 264–276.

Huang M.J., Eames P.C., Norton B., 2004. International Journal of Heat and Mass Transfer 47, 2715–2733.

Huang M.J., Eames P.C., Norton B., 2006. Solar Energy 80, 1121–1130.

Huang M.J., Eames P.C., Norton B., 2007. Heat Transfer Engineering 28, 31-37.

Huang M.J., Eames P.C., Norton B., Hewitt N.J., 2011. Solar Energy Materials & Solar Cells 95, 1598–1603.

Indartono Y.S., Suwono A., Pratama F.Y., 2014. International Journal of Low-Carbon Technologies 0, 1-5.

Kamkari B., Groulx D., 2018. Experimental Thermal and Fluid Science 97, 94–108.

Kant K., Shukla A., Sharma A., Biwole P.H., 2016. Solar Energy 140, 151–161.

Kaplani E., Kaplanis S., 2014. Solar Energy 107, 443–460.

Khanna S., Newar S., Sharma V., Reddy K.S., Mallick T.K., 2019. Energy Conversion and Management. 180, 1185-1195.

Khanna S., Sharma V., Singh S., Kedare S.B., 2016. Applied Thermal Engineering 103, 323–332.

Khanna S., Reddy K.S., Mallick T.K., 2017. Energy 133, 887-899.

Khanna S., Sharma V., 2015. Energy 93, 1788–1803.

Khanna S., Sharma V., 2016. Journal of Solar Energy Engineering 138, 011010.

Khanna, S., Singh, S., Kedare, S.B., 2014. Energy Procedia 48, 123–129.

Khanna S., Reddy K.S., Mallick T.K., 2018a. Energy Conversion and Management 166, 590–601.

Khanna S., Reddy K.S., Mallick T.K., 2018b. Solar Energy 174, 593–605.

Khanna S., Reddy K.S., Mallick T.K., 2018c. International Journal of Thermal Sciences. 130, 313-322.

Khanna S., Reddy K.S., Mallick T.K., 2018d. Solar Energy 163, 591-599.

Khanna S., Reddy K.S., Mallick T.K., 2018e. AIP Conference Proceedings 2012, 080007.

Khanna S., Sundaram S., Reddy K.S., Mallick T.K., 2017. Applied Thermal Engineering 127, 559–565.

Kibria M.A., Saidur R., Al-Sulaiman F.A., Aziz M.M.A., 2016. Solar Energy 124, 114–123.

Lu W., Liu Z., Flor J.F., Wu Y., Yang M., 2018. Applied Energy 225, 696-709.

Ma T., Zhao J., Li Z., 2018. Applied Energy 228, 1147-1158.

Park J., Kim T., Leigh S.B., 2014. Solar Energy 105, 561–574.

Preet S., Bhushan B., Mahajan T., 2017. Solar Energy 155, 1104–1120.

Sathe T. M., Dhoble A.S., 2018. Journal of Renewable and Sustainable Energy 10, 043704.

Sharma S., Micheli L., Chang W., Tahir A., Reddy K.S., Mallick T.K., 2017. Applied Energy 208, 719–733.

Sharma V., Khanna S., Nayak J.K., Kedare S.B., 2016. Energy 94, 633–653.

Siyabi I. Al, Khanna S., Mallick T., Sundaram S., 2018a. AIP Conference Proceedings 2012, 080001.

Siyabi I. Al, Khanna S., Mallick T., Sundaram S., 2018b. Energies 11 (7), 1629.

Su D., Jia Y., Alva G., Liu L., Fang G., 2017. Energy Conversion and Management 131, 79–89.

Su Y., Zhang Y., Shu L., 2018. Solar Energy 159, 777–785.

Waqas A., Jie J., Xu L., 2017. Journal of Renewable and Sustainable Energy 9, 053504.

Zhang N., Yuan Y., Cao X., Du Y., Zhang Z., Gui Y., 2018. Advanced Engineering Materials 20, 1700753.

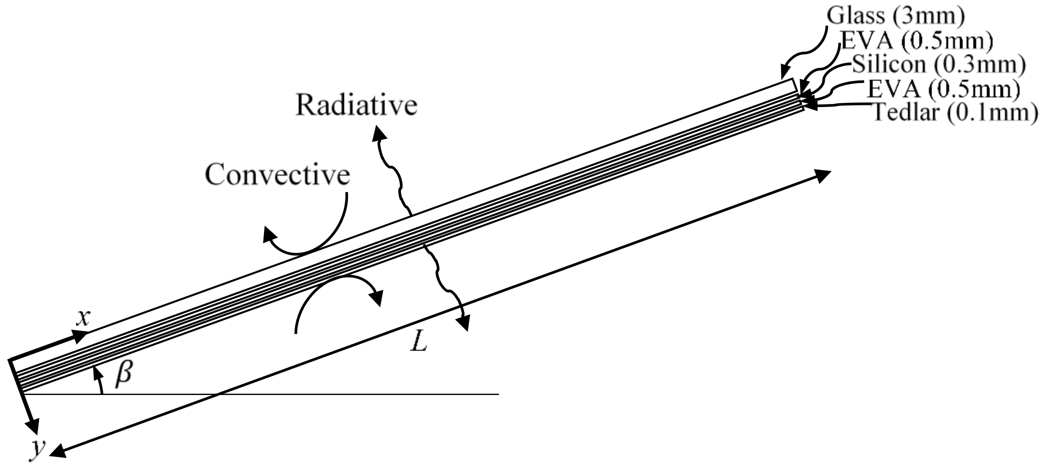

(a) PV

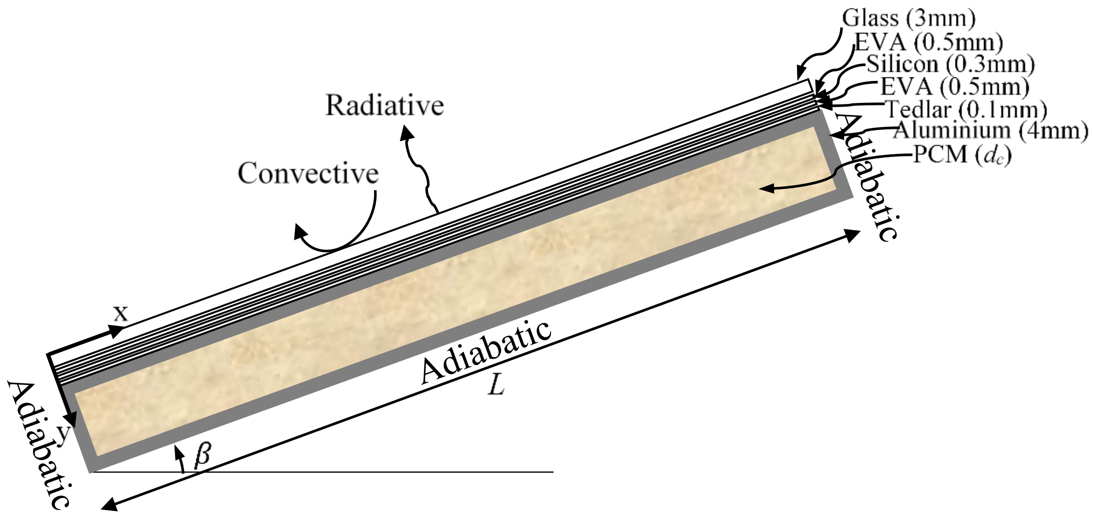

(b) PV-PCM

Fig. 1 PV and PV-PCM studied in current work

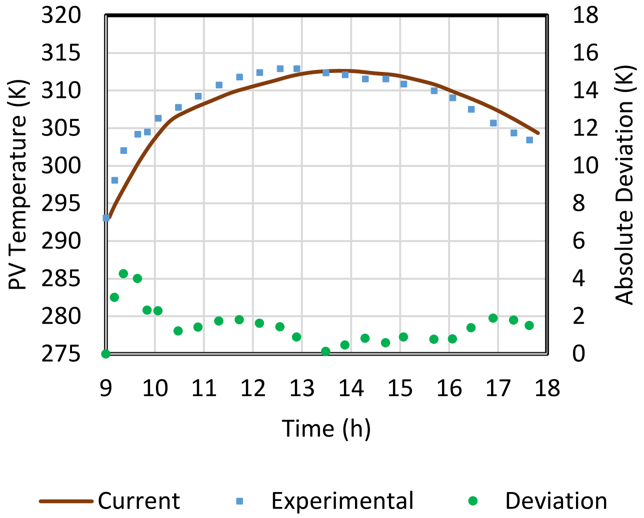

322

323 *Figure 2 Comparison of computed and experimental values (Hasan et al., 2015)*

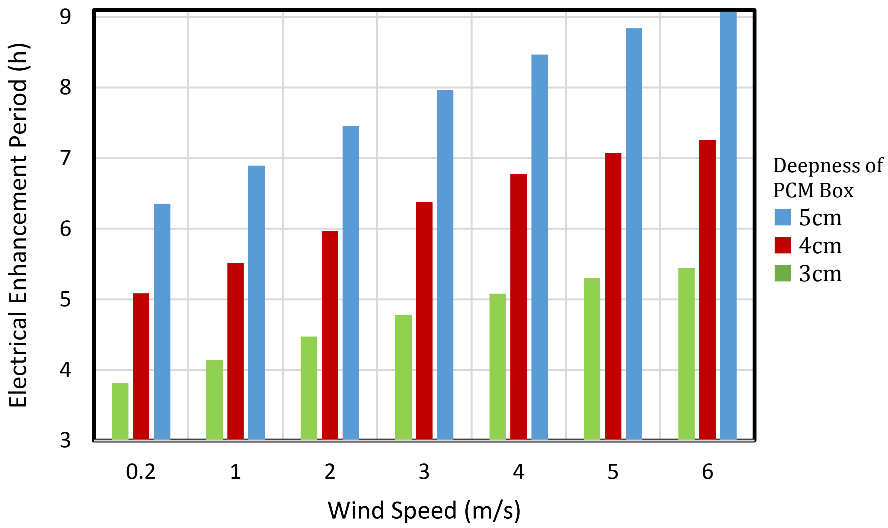

Figure 3 Electrical Enhancement Period of PV for a span of wind speed and deepness of PCM box

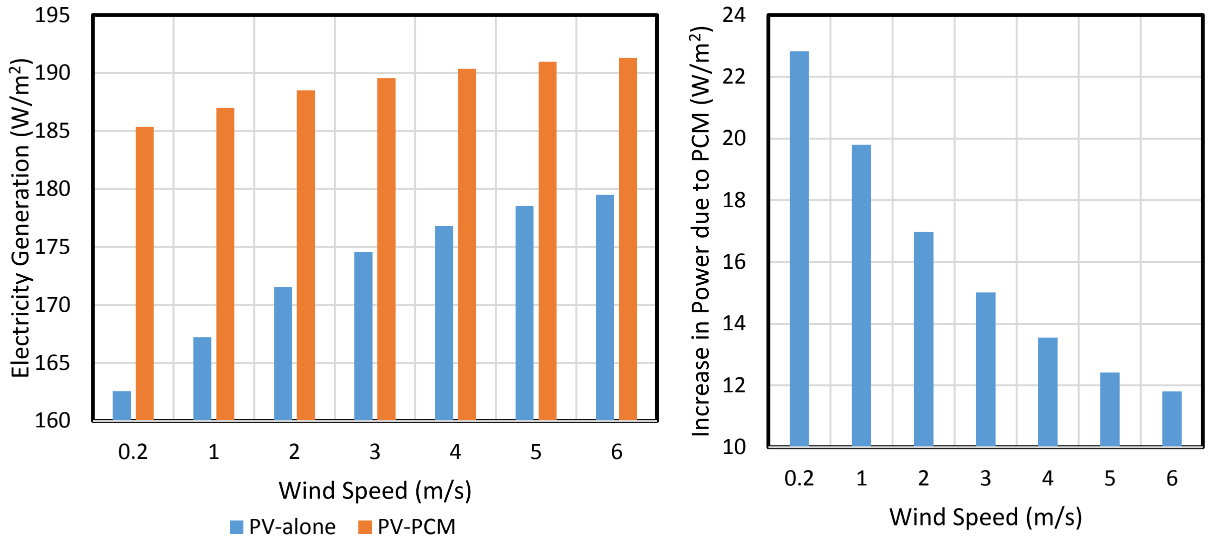

Figure 4 Electricity generation and increase in power achieved using PCM for a span of wind speed

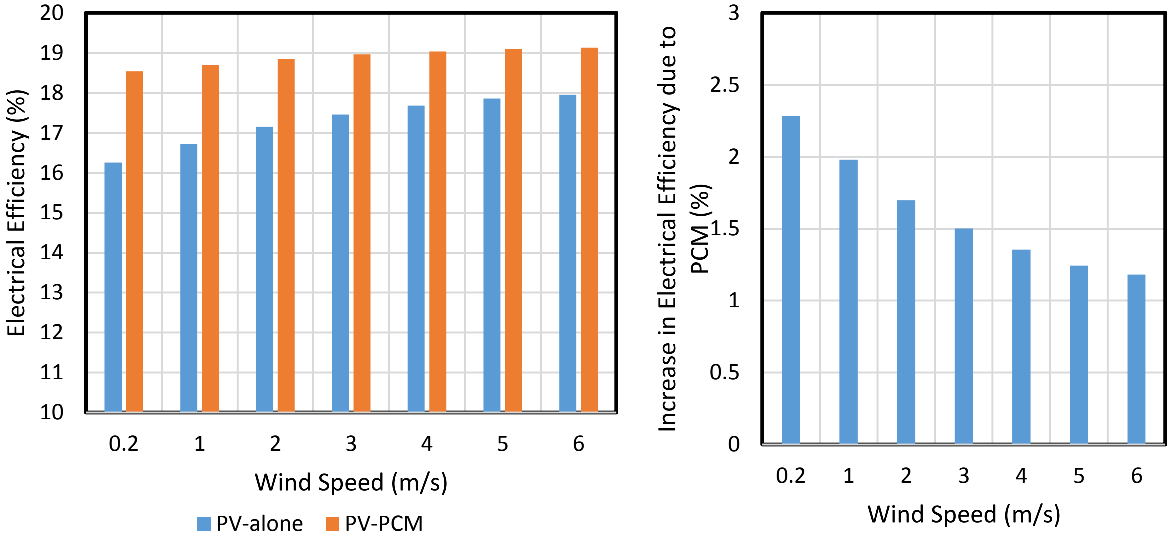

Figure 5 Electrical Efficiency and increase in electrical efficiency achieved using PCM for a span of wind speed

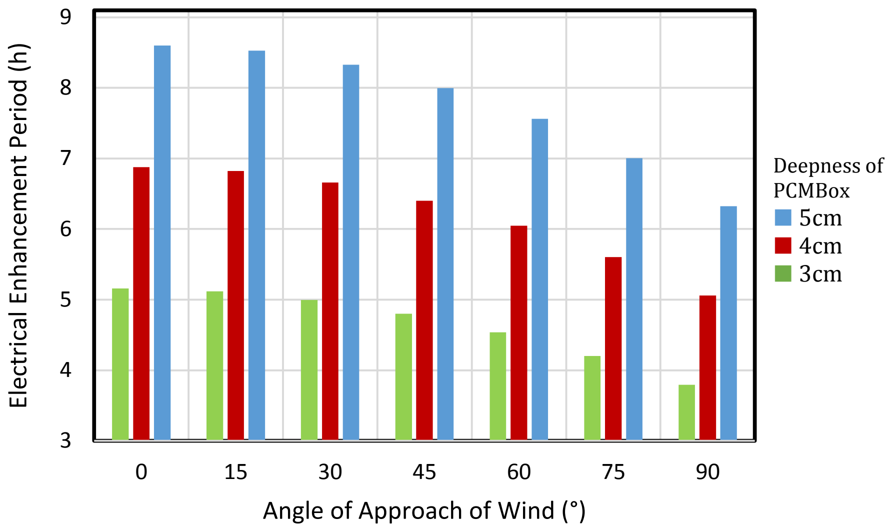

Figure 6 Electrical Enhancement Period of PV for a span of angle of approach of wind and deepness of PCM box

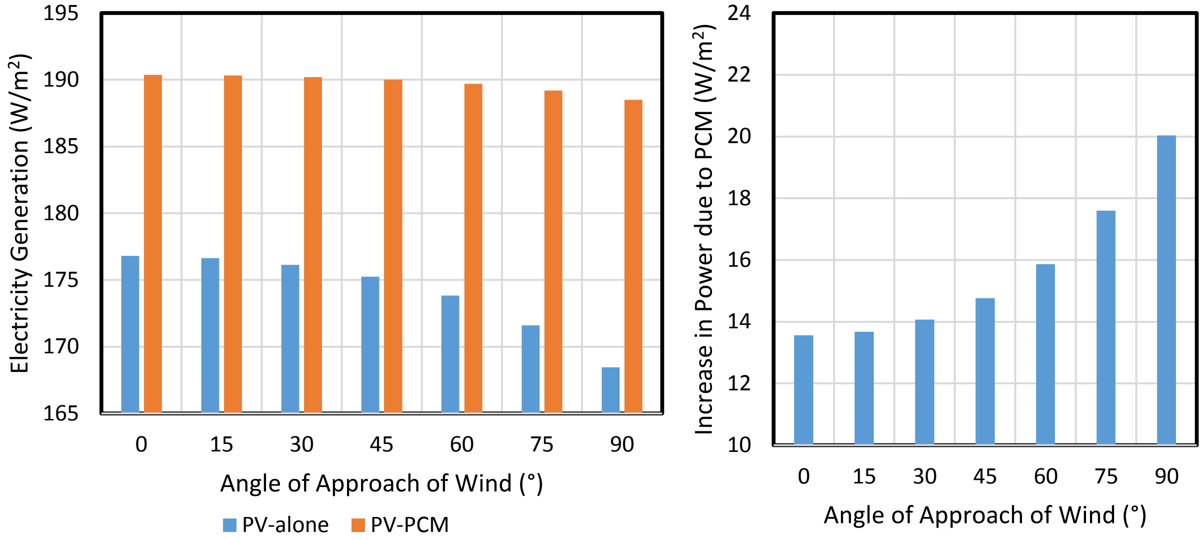

Figure 7 Electricity generation and increase in power achieved using PCM for a span of angle of approach of wind

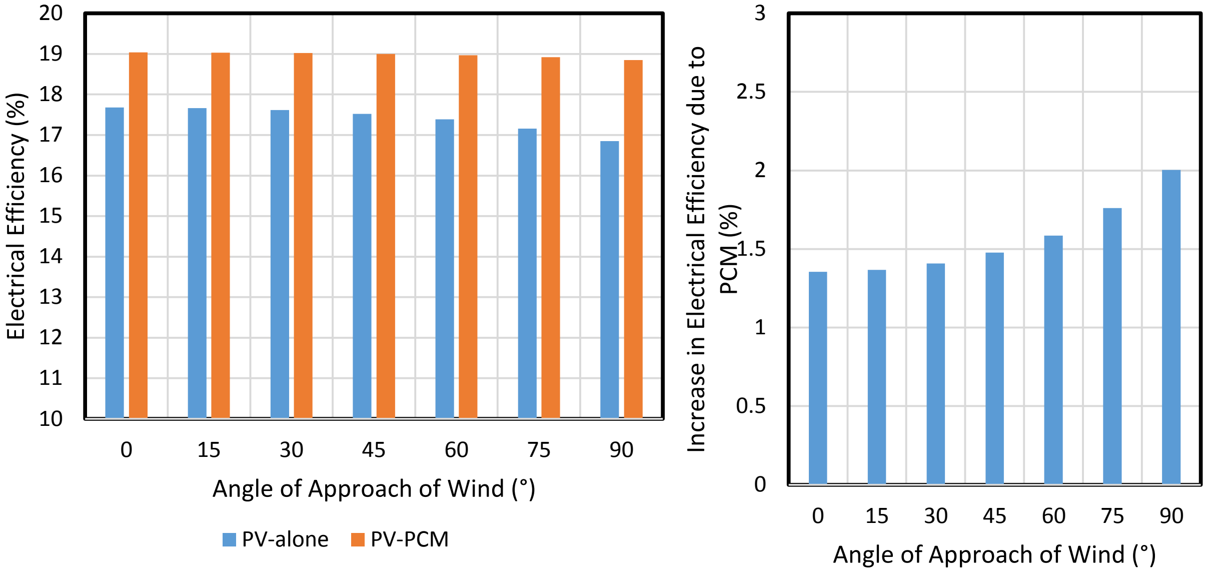

Figure 8 Electrical Efficiency and increase in electrical efficiency achieved using PCM for a span of angle of approach of wind

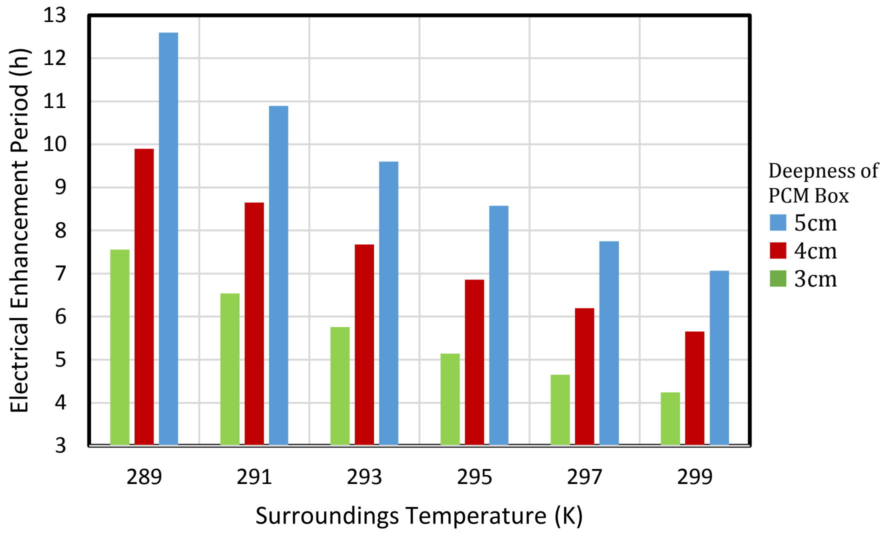

Figure 9 Electrical Enhancement Period of PV for a span of surroundings temperature and deepness of PCM box

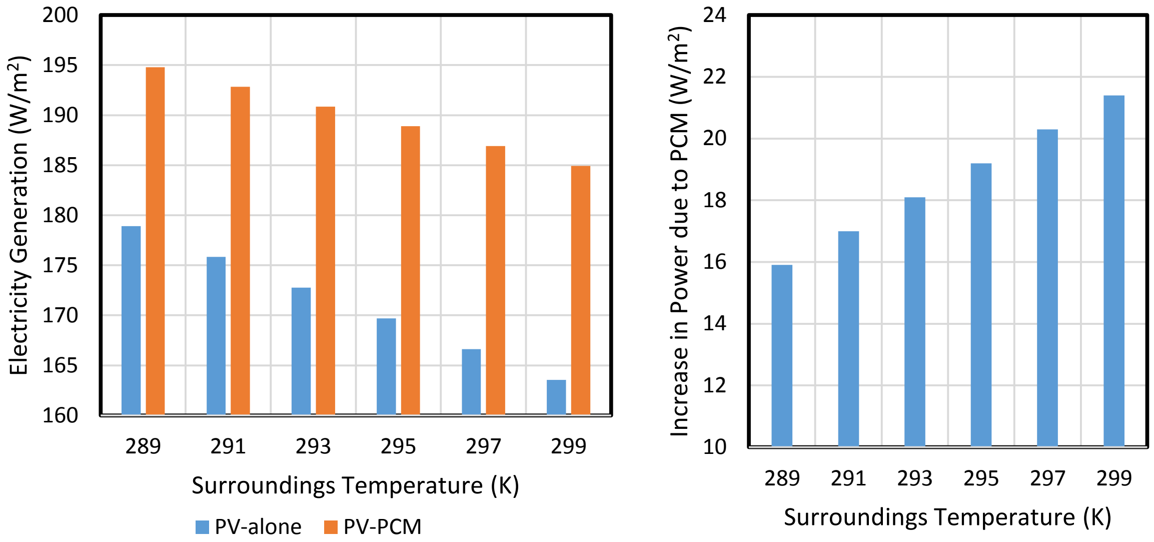

345

346 *Figure 10 Electricity generation and increase in power achieved using PCM for a span of*
347 *surroundings temperature*

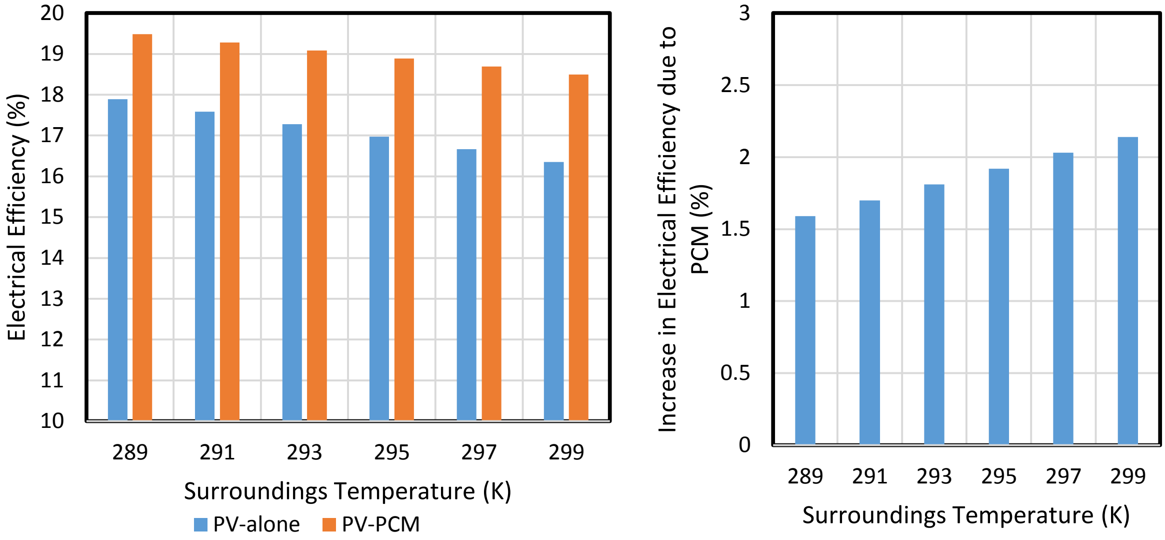

Figure 11 Electrical Efficiency and increase in electrical efficiency achieved using PCM for a span of surroundings temperature

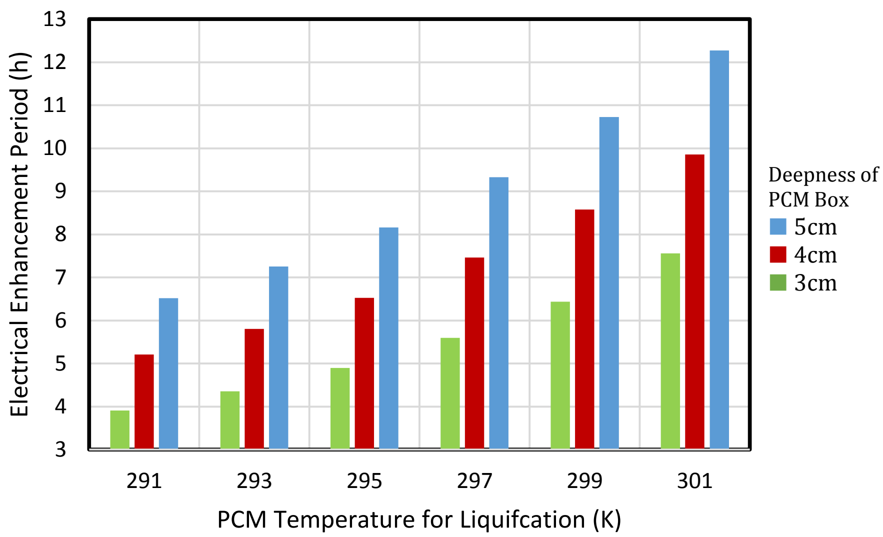

Figure 12 Electrical enhancement period of PV for a span of PCM liquification temperature and deepness of PCM box